CAVITATION INCEPTION ON THE I.T.T.C. STANDARD HEAD FORM

FINAL REPORT

U. S. Naval Ordnance Test Station
Contract N60530-12258

HYDRODYNAMICS LABORATORY

KÁRMÁN LABORATORY OF FLUID MECHANICS AND JET PROPULSION

CALIFORNIA INSTITUTE OF TECHNOLOGY

PASADENA, CALIFORNIA

Hydrodynamics Laboratory
Kármán Laboratory of Fluid Mechanics and Jet Propulsion
California Institute of Technology
Pasadena, California

CAVITATION INCEPTION ON THE I.T.T.C. STANDARD HEAD FORM

FINAL REPORT
U. S. Naval Ordnance Test Station
Contract N60530-12258

by

A. J. Acosta
and
H. Hamaguchi

Report No. E-149.1

March 1967

California Institute of Technology
Division of Engineering and Applied Science
Pasadena, California

CAVITATION INCEPTION ON THE I.T.T.C. STANDARD HEAD FORM

by

A. J. Acosta and H. Hamaguchi

Final Report

U. S. Naval Ordnance Test Station Contract N60530-12258

Abstract: Cavitation inception measurements were made on the I.T.T.C. Standard Head Form over a range of speeds and dissolved air content. The results were similar to those observed in other water tunnels with resorbers. Cavitation inception indices were observed as low as 0.4 as compared with the minimum calculated pressure coefficient of 0.6. As in previous measurements a pronounced velocity scale effect was observed.

Nomenclature

K	-	cavitation index based upon vapor pressure $(p_o - p_v)/\rho V^2/2$
p_o	-	tunnel static pressure
p_t	-	total pressure
p_v	-	vapor pressure
V	-	tunnel speed
a/a_s	-	ratio of dissolved air content to saturation value at one atmosphere
ρ	-	density

Introduction:

The present experimental program was undertaken as a part of the program of comparative cavitation inception tests initiated by the Swedish State Shipbuilding Experimental Tank in 1963 (Ref. 1). A large amount of data has been compiled in this program with the cooperation of the International Towing Tank Committee. This information is compiled and presented in Reference 2. The intent of the comparative program was

to observe differences in the determination of cavitation inception between various types of water tunnel facilities. As of the present time, as discussed in Reference 2, approximately 17 different cavitation tunnel configurations have been used to make these cavitation inception determinations. The present results are intended to add to the body of knowledge already gained and are intended specifically to make comparisons of cavitation inception measurements in the High Speed Water Tunnel at the California Institute of Technology, which has a resorber, and the Vertical Open Jet Water Tunnel at the Naval Ordnance Test Station, Pasadena, which does not have a resorber. In these present tests the same test object has been used by both the Naval Ordnance Test Station and the California Institute of Technology in order to avoid geometric scale problems that can arise when different models are used in different facilities. The Naval Ordnance Test Station investigation (Ref. 3) will be published in the near future and the present study is concerned mainly with the experimental findings at the California Institute of Technology.

As discussed in Reference 1, the I.T.T.C. headform selected for the comparison tests is a modified ellipsoidal body of revolution consisting of a tangent ellipse one-half diameter in length and having a flat face with a diameter of one-half the body diameter. Wherever possible, the techniques and procedures suggested in Reference 1 were followed.

Experimental Procedure: The test body (supplied by the Naval Ordnance Test Station) was fabricated from 303 stainless steel and was 1.755 inches in diameter. It was mounted in the circular working section of the High Speed Water Tunnel on a sting support which was seven diameters downstream of the nose. A photograph of the tunnel working section with test body installed is shown in Figure 1. The sting support consisted of a three-legged spider containing a socket fixture into which the test body was fixed. This mounting provided a rigid support for the model and during all tests no vibration or movement of the model could be discerned.

The working section has a diameter of 14 inches so that the test body occupied less than 2 percent of the throughflow area. Nevertheless, this

amount of blockage and the boundary layer built up along the walls of the test section which presumably can be modified by the presence of the body necessitated a careful calibration of the test section in order to report tunnel speeds and cavitation numbers. This procedure is outlined and discussed in Appendix I. After the model was installed, measurements were made to determine the possible misalignment between the axis of the model and the tunnel axis. It was found that these two directions differed by an angle of 0.17degrees. Small though this was, it did cause an observable and systematic difference in the observed cavitation on the two sides of the test body.

In carrying out the observations of cavitation inception the model was illuminated by stroboscopic light at various frequencies; 20 flashes per second was a typical value. No attempts were made to determine the onset of cavitation by acoustic means even though these were available. A camera was set up on the side of the tunnel opposite the observer, and after cavitation inception had taken place a photograph of the visible cavitation was taken by means of the usual arc discharge lamp. The amount of the dissolved air in the working section of the tunnel was determined at the start and close of each day of operation. Before each day of operation the surface of the test body was cleaned with acetone, as is suggested in Reference 1.

With the model installed in the tunnel and the tunnel filled with water from the reservoir, the operating speed would be established and the test section pressure would be lowered - approximately at the rate of one inch of mercury every 30 seconds - until the first signs of cavitation on the model began. When cavitation did take place all valves connecting manometers to the tunnel were closed and the data point was recorded. The pressure was then raised to make the cavitation disappear and the process was repeated. Several, usually three, data points were taken for each tunnel speed and air content. Sometimes, but not always, these inception point observations were interspersed with determinations of the desinent cavitation point - that is, the point at which cavitation disappears. While most cavitation inception and desinent measurements were made on the operator's side of the tunnel, some similar measurements were made on the camera side of the tunnel. As previously mentioned,

these all are systematically higher, though by a small amount.

The amount of air dissolved in the water was lowered from its saturation level by operating the tunnel at low pressure for extended periods of time; the cavitation in the test section then liberated dissolved air which was then periodically bled off. Typically after two days of such operations, the air content can be lowered from its saturation value to approximately 50 percent of that value. Substantial reductions lower than this amount are probably not feasible in this water tunnel due to the large volume of water concerned (approximately 70,000 gallons).

Appearance of Cavitation: At this stage we would like to describe the cavitation that appears on the I.T.T.C. test body in the High Speed Water Tunnel. Reference 1 contained a definition of cavitation inception which was dependent upon the number of inception bubbles which were observed on the test body. In practically all of the present tests no free bubbles, or very few, in the working section upstream of the test body were observed even up to speeds of 20 meters per second. This is in contrast to many other water tunnels in which a copious number of free air bubbles are plainly evident - for example, the Naval Ordnance Test Station Vertical Water Tunnel. Furthermore, as the point of cavitation inception on the body is reached, no minute traces of cavitation bubbles were seen on the I.T.T.C. test body. In practically every case when cavitation inception occurred, it took place suddenly and abruptly in the form of a small band all around the nose of the body. This appearance was characteristically abrupt rather than gradual and there were no 'precursors' suggesting that cavitation inception was imminent. With this type of inception there was a correspondingly sudden increase in the auditory sound level from the tunnel. This type of cavitation, which we will term "band" cavitation, is illustrated in Figure 4 over a wide range of tunnel speeds. At the highest speeds used in these tests (approximately 20 meters per second), another form of cavitation inception appeared which at first was thought to be due to small particles or debris in

the water attaching themselves to the surface. This view was reinforced by the observation that if the tunnel were stopped or if the pressure were raised sufficiently to cause the disappearance of this form of cavitation, it would not always re-appear upon lowering the pressure again. Close inspection, however, revealed that in every case of this type of cavitation no debris could be observed on the nose of the body and we came to the conclusion that this type of cavitation was inherent at higher speeds. A photograph of this type of cavitation described is shown in Figure 5. There it can be seen that the cavitation commenced at a pinpoint or spot and spread in the form of a V rather like a wake. For want of a better term we will call such cavitation "spot" cavitation. Unlike the band cavitation, spot cavitation occurred erratically, at consistently higher pressures, and further forward on the nose of the body. In what follows we decribe primarily the onset and disappearance of the band type of cavitation as it was the more prevalent and more repeatable and it was the only form that occurred consistently at lower speeds, say lower than the 15 meters per second.

Results: The principal results of this experiment are summarized in Figures 2a, b, c and d and Figure 3. In the first of these figures are plotted the inception cavitation number versus tunnel speed in meters per second for the various air contents used. In these graphs the tunnel speed and the cavitation index have been computed by taking no account of any tunnel blockage by the model. As shown in Appendix 1 the change in wall pressure due to the presence of the model is small and in fact agrees in order of magnitude with the changes in pressure distribution as calculated in Reference 4. Also shown in Figure 2a is the mean line of the experimental results from two other water tunnels having resorbers; this information is abstracted from Reference 2.

In Figure 2a it is seen that there is a fairly wide spread of cavitation inception at a particular speed - for example, depending upon air content the range in cavitation inception index can vary as much as 0.04. Not all of this is scatter, however, and consistent trends with air content ratio are observable. Also shown on Figure 2a are observations of the

cavitation desinent point - that is, when the cavitation disappears, for various speeds. These points are shown offset +0.5 meters per second in order not to be confused with the inception points. As a general rule the desinent points are somewhat higher than the inception points. It is also evident that there is a systematic difference between the two sides of the model, as mentioned in the previous section. Owing to the small misalignment of the model with the tunnel axis, inception on the camera side of the tunnel appeared somewhat before inception on the operator side. It is difficult to be precise about this, but there appear to be systematic differences on the order of 0.01 K.

For any one air content and speed the variation in the cavitation inception point judged by the scatter of the data points is about 0.025. All of these data points were averaged for various air contents and are shown in Figure 2b for the three air contents used - namely, a/a_s = 0.55, 0.8 and 1.3. At the lower operating speeds with the inception indices of these tests, the tunnel working section ambient pressure was usually less than atmospheric pressure. To obtain the lower two air content levels, it was necessary to remove dissolved air from the working fluid by operating the tunnel at reduced pressure as previously described. In order to obtain the highest air content used, especially at the highest velocities for the tunnel, it was necessary to inject air into the working section in the form of free bubbles and circulate these bubbles for many minutes in order to mix thoroughly this air with the working fluid. When this had been done and the tunnel run at the lower speed such as 12 meters per second, we then observed a number of discrete free air bubbles in the working section upstream of the model. The form of the cavitation at inception was still much as it was for the lower air contents, namely the band form. The inception points, however, are systematically higher by approximately 0.02 K. Whether this larger value of inception cavitation index is due to the excess amount of dissolved air present or to the presence of the free bubbles themselves, we cannot determine at this time. There is little noticeable effect of air content for the lower two values. The present observations are, however, below those as measured in open circuit water tunnels.

In the present experiments it seemed reasonably likely that the source of nuclei which contributed to the inception of cavitation probably originated on the body rather than in the bulk of the fluid judging by the lower values of cavitation index observed and by the freedom from free air bubbles in the working section. It was thought that a change in the surface condition of the test body might affect the inception of cavitation if it did alter (either increase or diminish) the supply of surface nuclei. A preliminary attempt to do this was carried out as follows: The nose of the test body was dipped into a mixture of a silicone fluid and solvent. The object of this procedure was to coat the surface of the body with a fluid which had the ability to dissolve a large amount of air - as silicone fluids are known to do. The actual fluid used was Dow Corning 703 and the solvent used to thin the silicone fluid was methyl ethyl ketone. The inception data obtained by this proecdure are shown in Figure 2c. The air content for all these experiments was approximately 0.55 normal saturation. These results are not entirely systematic nor conclusive, but what appeared to happen was as follows: After application of the silicone fluid which was highly saturated with air, free bubbles were observed to grow from the surface of the body at reduced pressure. It is presumed that these bubbles caused the inception observed, at the higher indices - approximately 0.47 - as can be seen in Figure 2c. When the coating became aged somewhat, the results were similar to those previously found in pure water. On the other hand, when the coating was old and evidently had become quite deaerated at the lower pressures, cavitation inception indices lower than those observed with pure water were found. For this latter case, the cavitation again appeared as a band except that due to the lower pressures at which the band was formed, the inception always took place more precipitously than with pure water.

The above explanation, tentative though it is, may explain why the data of Figure 2c are arranged into three groups - the higher for the bubble type inception, the middle which is typical of the pure water, and a lower envelope, so to speak, with band cavitation again. Desinent

measurements were also carried out with the silicone fluid coating and unlike the case of pure water, a wide range in this latter parameter was observed. These are shown in Figure 2d. Here we see desinent inception numbers as high as 0.5 but typically they are all higher than equivalent values observed with pure water alone.

As mentioned above, a photograph was taken for each of the different air contents and tunnel speeds. These photographs of necessity had to be taken at pressures slightly below the inception pressure. Measurements were also made on these photographs of the position at which cavitation originated. In the present experiments this was at the leading edge of the "band" which was the usual form of occurrence of the cavitation. The photographic setup was calibrated by photographing a measuring scale at the plane of the model. The location of the forward edge of the visible cavitation was measured with a travelling stage microscope and with the calibration factor determined. The axial distance downstream of the nose as a fraction of the diameter could be determined. These data are all summarized in Figure 3 for the various air contents used. As mentioned above, most of these data points are for the band type of cavitation. However, there are a few points shown for the "bubble" type cavitation inception observed on the experiments with the silicone fluid. From Figure 3 it can be seen that values of x/d for the bubble inception are about 0.28, whereas the great bulk of band type cavitation was observed at 0.45 diameters downstream of the nose. Incidentally this latter value is in the middle of the range of positions for cavitation inception observed at the National Physical Laboratory. Also shown for the sake of comparison on this figure are two data points of the spot type of inception which is shown in Figure 5. Interestingly enough, this type of cavitation starts at nearly the same location as that observed for the bubble inception with the silicone fluid. Hoyt in Reference 4 has computed that the position of the minimum surface pressure on the body is located 0.28 diameters downstream of the nose, the same as that observed for the spot and bubble inceptions. The positions observed both by us and by the National Physical Laboratory for the band cavitation occur significantly

downstream of the position of minimum pressure.

Both Figures 4 and 5 are photographs of the cavitation at pressures slightly below the cavitation inception value. In the first of these (Fig. 4) are shown a series of photographs over a range of speeds from approximately 25 feet per second (7.6 meters per second) to 60 feet per second (18.3 meters per second). The "band" of cavitation is clearly evident in each of these and in fact the form of the cavitation is pretty much the same over this range of speeds except that at the lowest speed minute traces of dissolved air can be seen leaving the downstream end of the cavity, whereas at the higher speed no such traces are seen. Similar photographs were taken at the lower air content ratio of 0.55, as shown in Figures 6a through 6d. It would be hard to say that these photographs are significantly different than those of Figure 4. Also shown in Figure 6e through 6h are photographs of the band cavitation with the silicone treatment on the model. No photographs are shown of the "bubble" inception previously discussed and in most important respects the band form of the cavitation is similar to that of Figures 6a through 6d and Figure 4. There may possibly be, however, a more prevalent trend for the "spot" type of inception already shown in Figure 5 to occur with the silicone treated body. It is interesting also to observe on these photographs the capillary waves which appear on these bands of cavitation. Another consistent feature is the streaks of "wetting" which appear to form fairly regularly around the periphery of the body. As far as the authors know, no explanation of these features has yet been put forward.

Acknowledgment: We would like to thank Dr. Richard Wade for his help in carrying out the experiments. Thanks are also due to Mr. J. Kingan, Mr. G. Lundgren, Mr. C. Eastvedt and Mrs. P. Henderson of the Hydrodynamics Laboratory staff for their support.

References:

1. Lindgren, H. and Johnsson, C. A., "A Proposal for Comparative

Cavitation Tests," DMK 64-1A, Swedish State Shipbuilding Experimental Tank, Goteborg, Sweden, December 1964.

2. Lindgren, H. and Johnsson, C. A., "Cavitation Inception on Head Forms, I.T.T.C. Comparative Experiments," S.S.P.A. Contribution to 11th International Towing Tank Conference.

3. Smith, H., "Cavitation Inception on the I.T.T.C. Standard Head Form," Naval Ordnance Test Station, Pasadena, California, under preparation.

4. Hoyt, J. W., "Wall Effect on I.T.T.C. Standard Head Shape Pressure Distribution," Contribution to 11th International Towing Tank Conference.

List of Captions

Fig. 1 - Experimental set-up in the High Speed Water Tunnel for testing the Swedish head form.

Fig. 2 - Cavitation inception on the I.T.T.C. standard head form for various velocities, air contents and surface conditions.

(2a) Inception and desinent velocities for air content ratios of a/a_s = 0.55, 0.8 and 1.3 versus velocity.

(2b) Average values of inception for air content ratios of a/a_s = 0.55, 0.8 and 1.3.

(2c) Inception at an air content ratio of a/a_s = 0.55 with the head form dipped into a solution containing Dow Corning 703 silicone oil.

(2d) Same as 2c except that desinent coefficients are measured.

Fig. 3 - Longitudinal position of the first appearance of cavitation versus velocity for the I.T.T.C. head form.

Fig. 4 - A series of photographs showing cavitation. Air content ratio a/a_s = 0.8.

Fig. 5 - Another type of cavitation attachment at higher velocities. Air content ratio a/a_s = 0.8.

Fig. 6 - A series of photographs showing cavitation on the I.T.T.C. head form at an air content ratio of a/a_s = 0.55.

(6a - d) Surface cleaned with acetone.

(6e - h) Surface dipped in silicone solution.

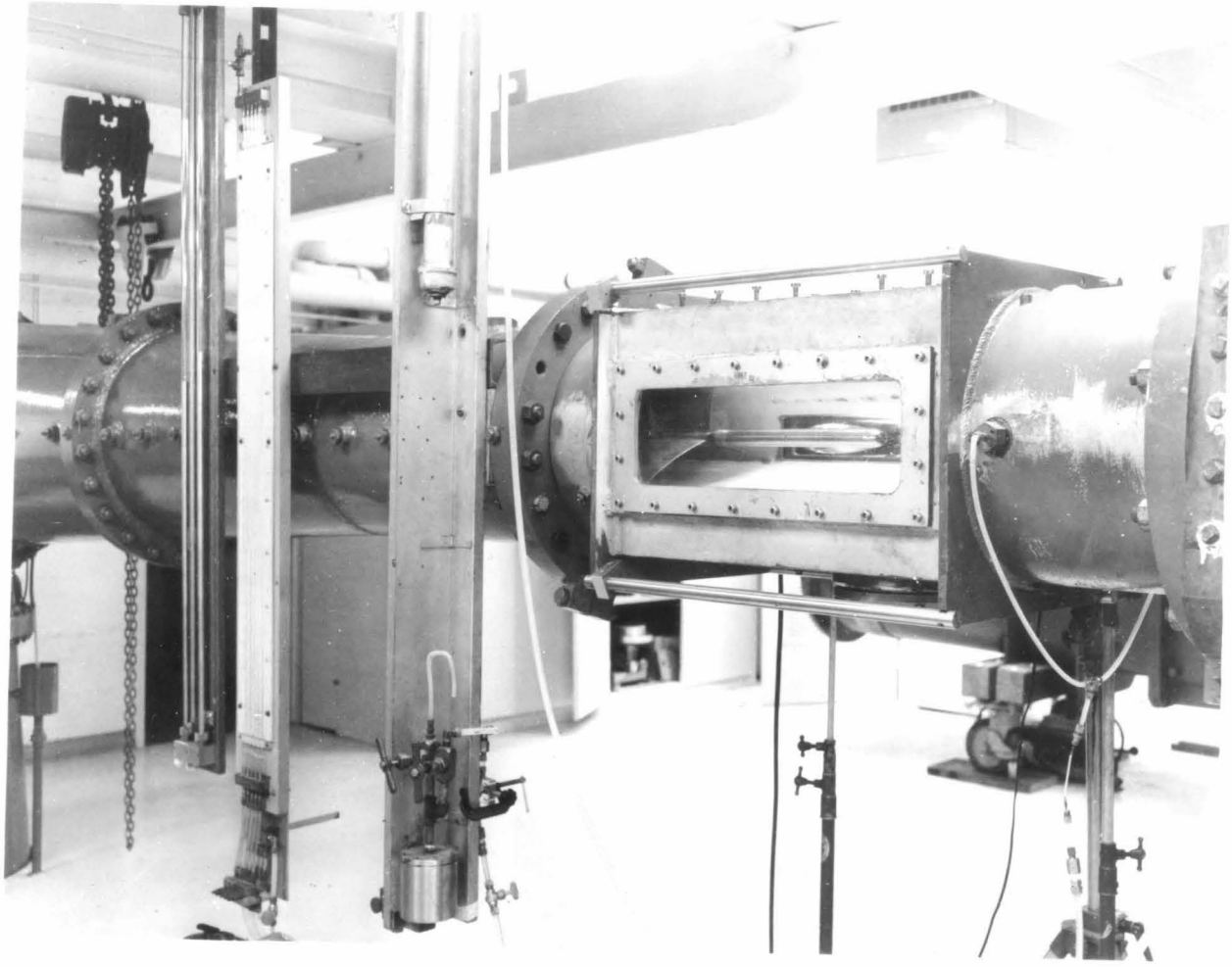

Fig. 1 - Experimental set-up in the High Speed Water Tunnel for testing the Swedish Headform.

INCEPTION & DESINENT - SWEDISH HEADFORM

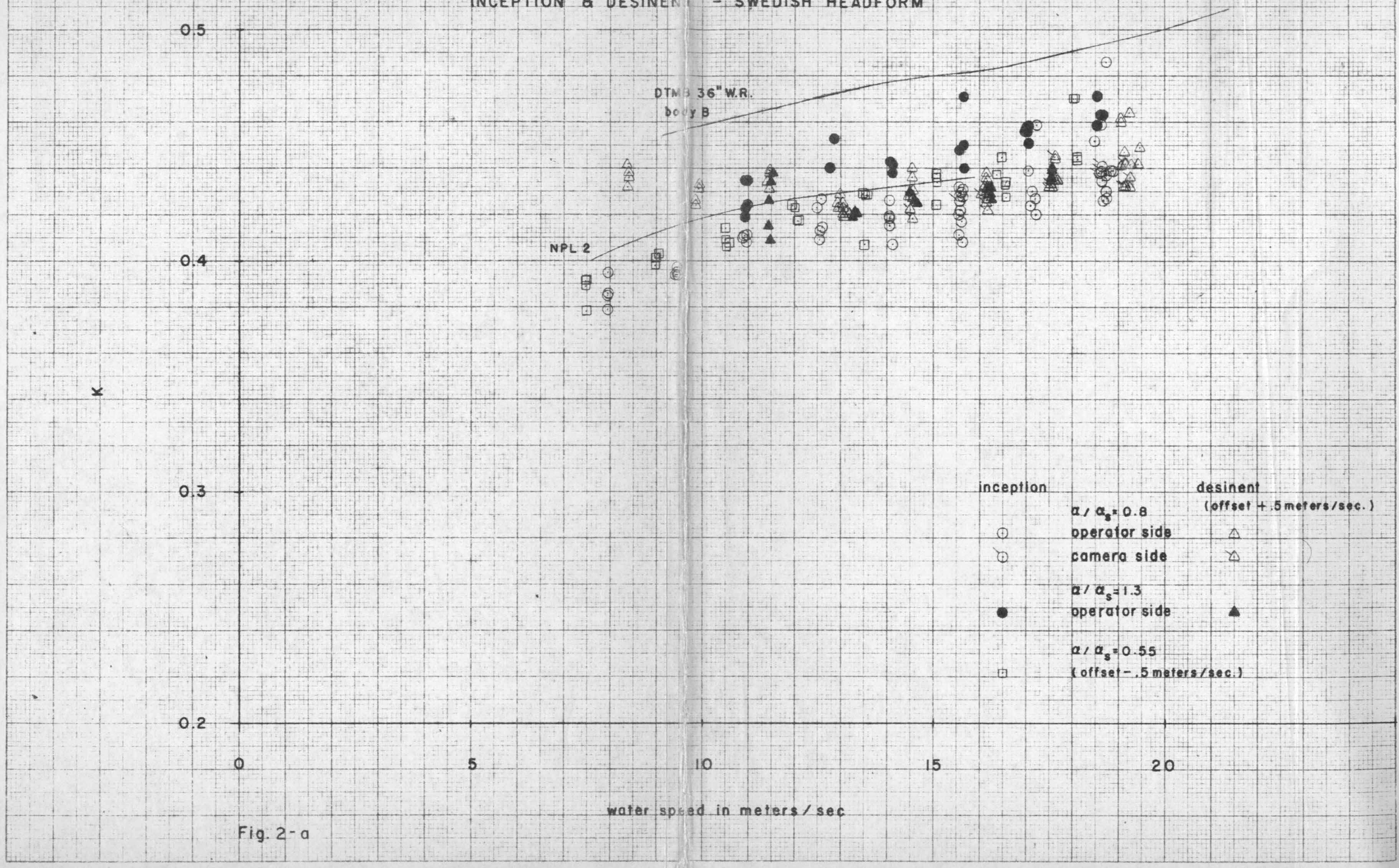

Fig. 2-a

AVERAGE INCEPTION - SWEDISH HEADFORM

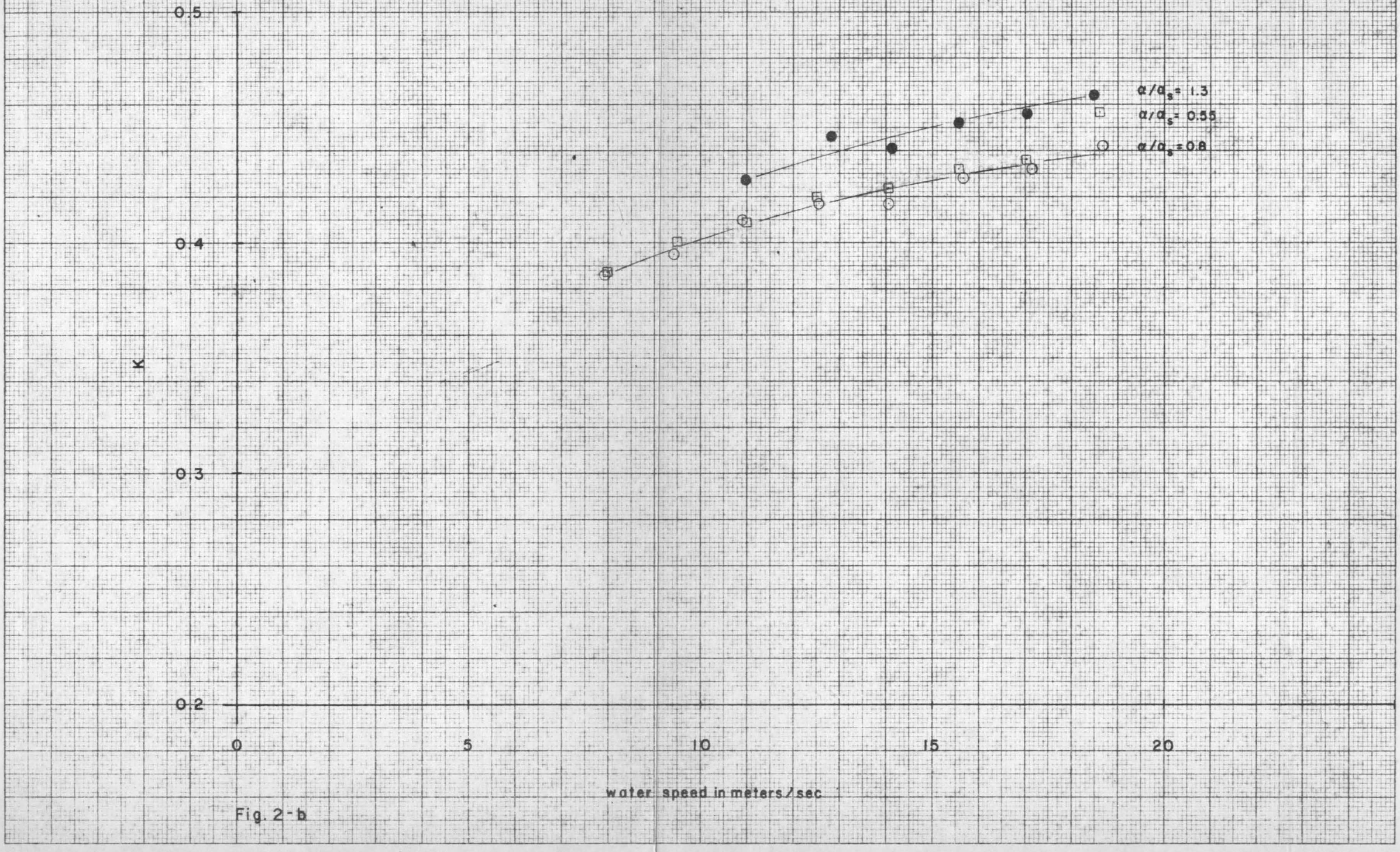

Fig. 2-b

INCEPTION - SWEDISH HEADFORM

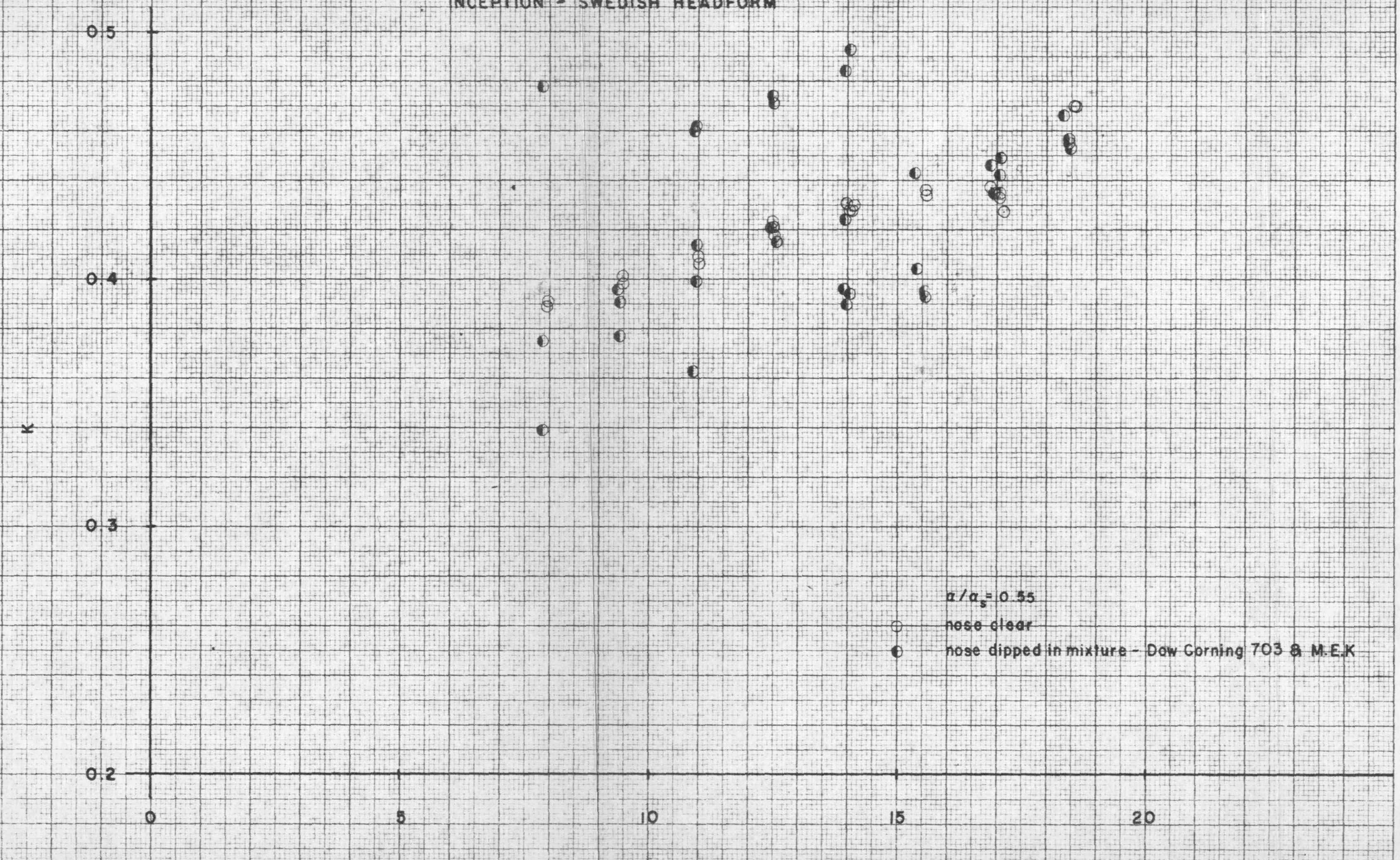

Fig. 2 - c

DESINENT - SWEDISH HEADFORM

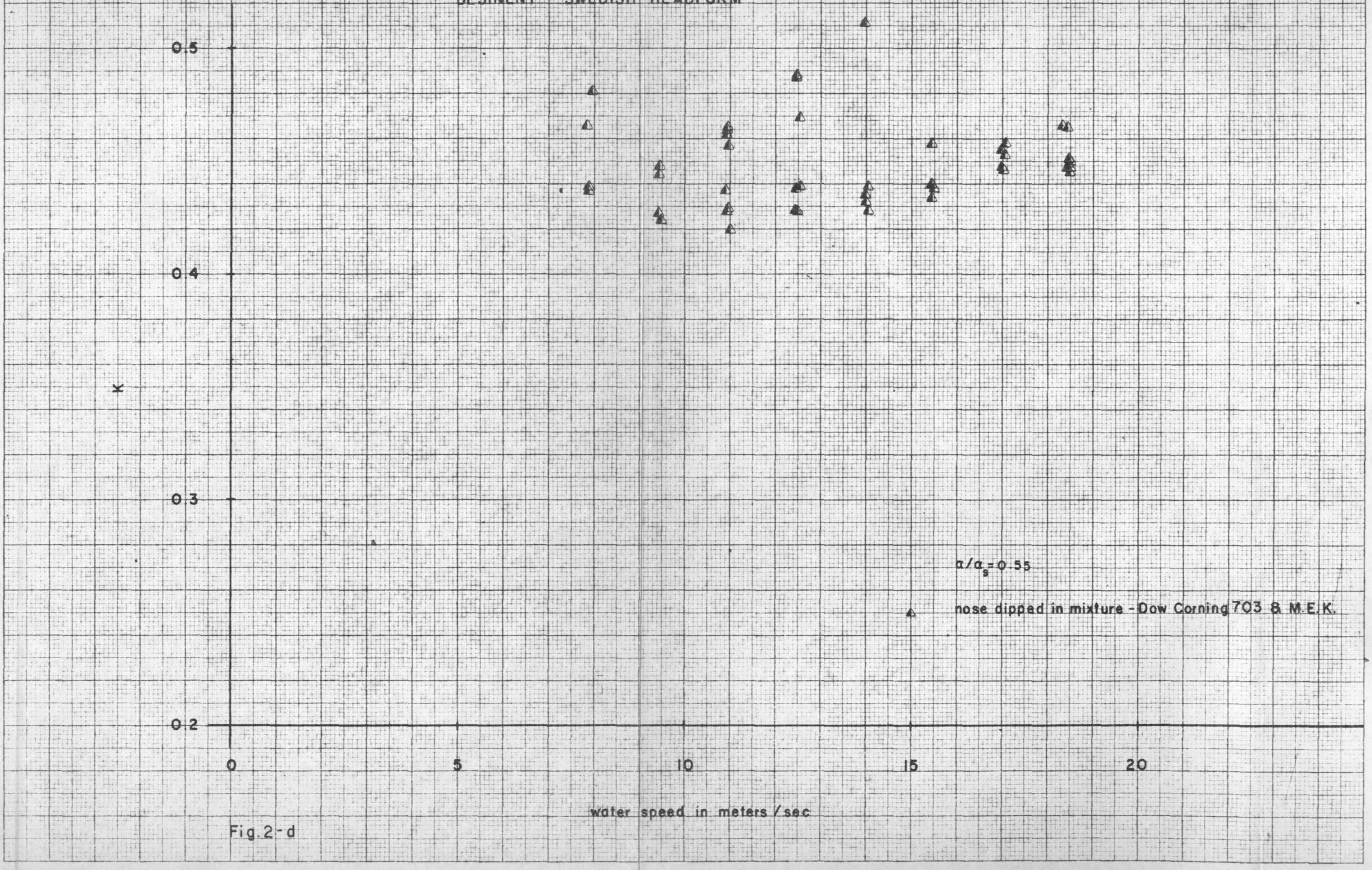

Fig. 2-d

LONGITUDINAL POSITION OF CAVITATION

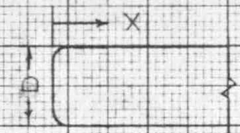

Fig. 3

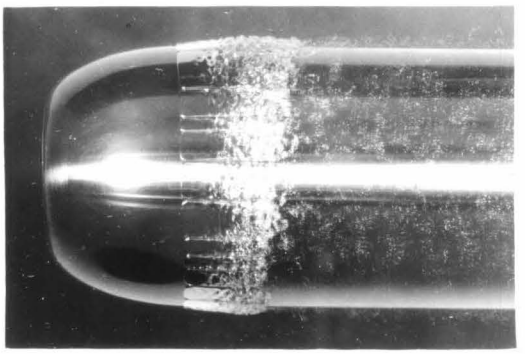

(a) V = 25.6 fps, K = 0.395

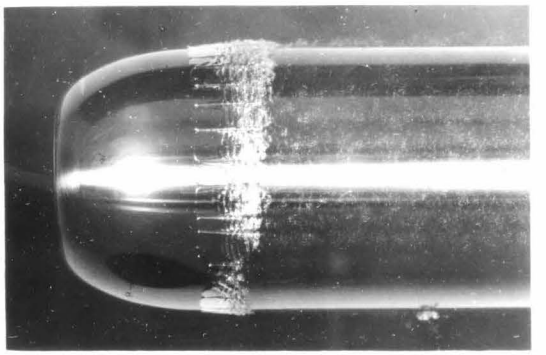

(b) V = 31.2 fps, K = 0.403

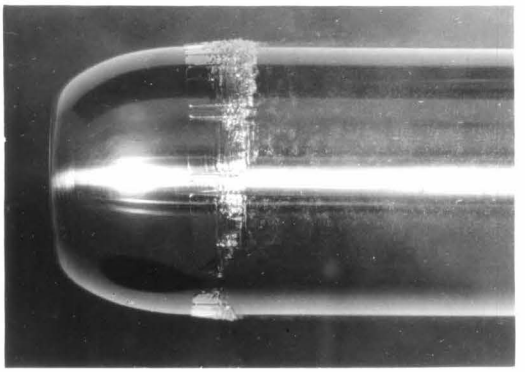

(c) V = 35.9 fps, K = 0.411

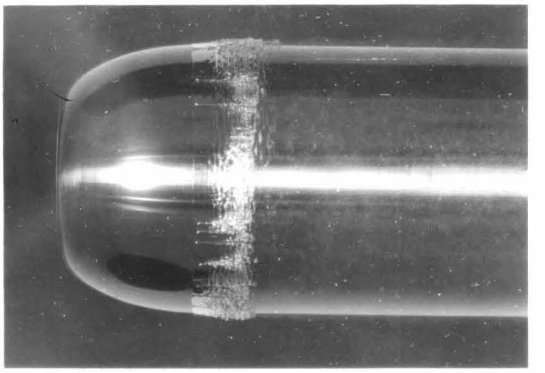

(d) V = 41.3 fps, K = 0.420

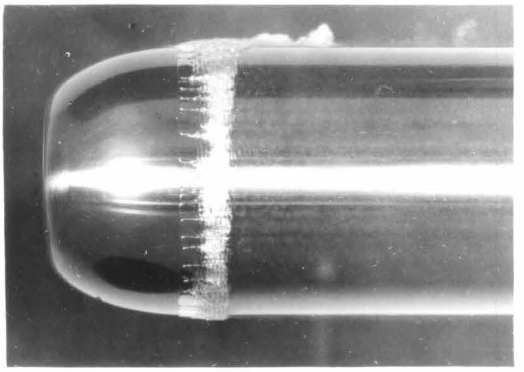

(e) V = 51.3 fps, K = 0.430

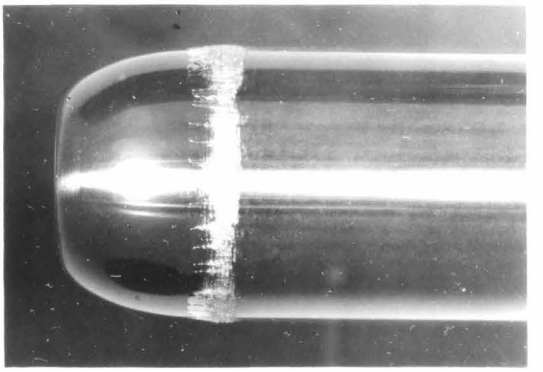

(f) V = 60.7 fps, K = 0.447

Fig. 4 - A series of photographs showing cavitation.
Air content ratio $a/a_s = 0.8$.

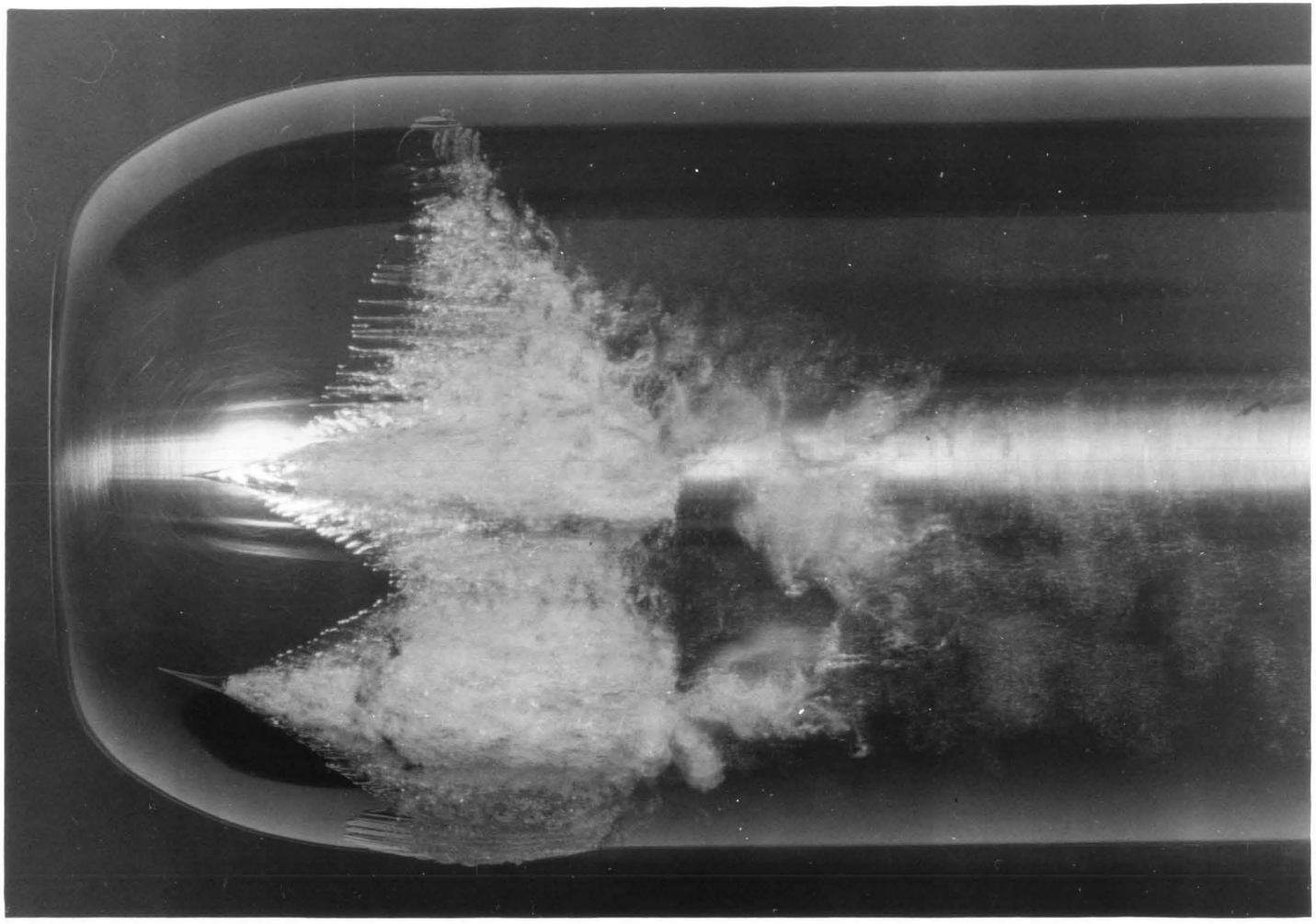

Fig. 5 - Another type of cavitation attachment at higher velocities.
Air content ratio $a/a_s = 0.8$.

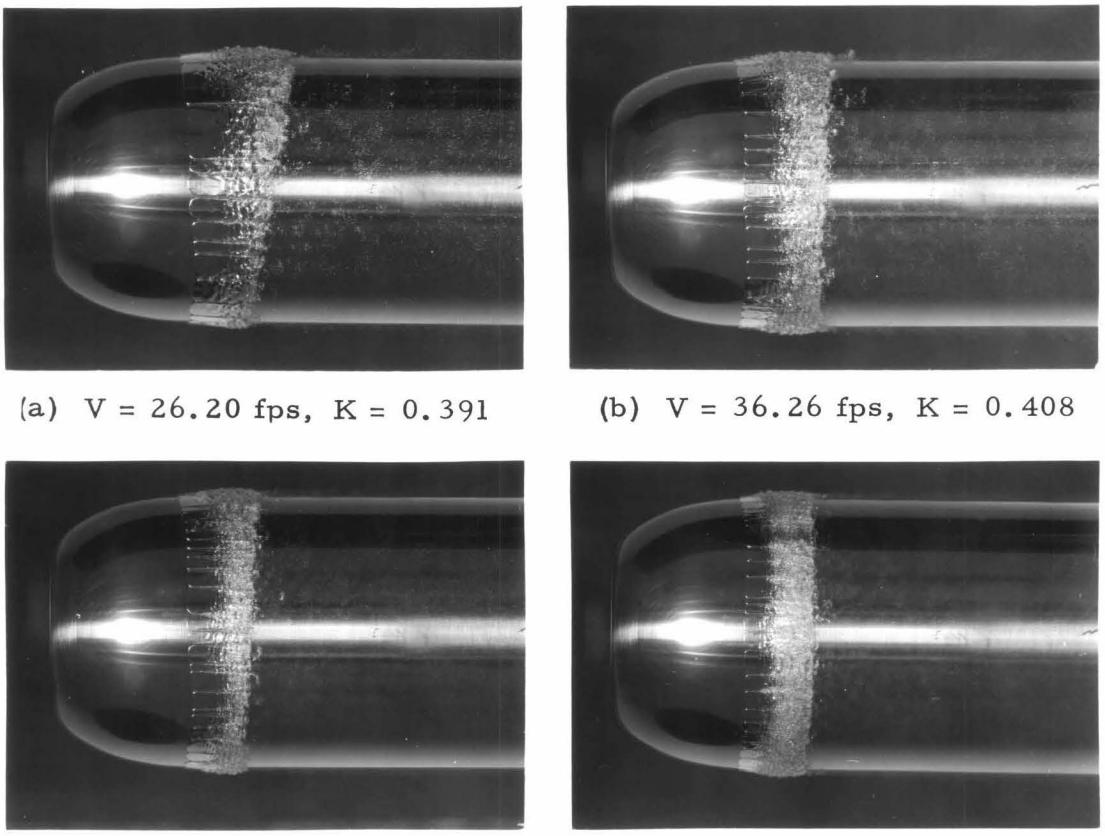

(a) V = 26.20 fps, K = 0.391

(b) V = 36.26 fps, K = 0.408

(c) V = 41.25 fps, K = 0.417

(d) V = 56.08 fps, K = 0.436

Fig. 6 - A series of photographs showing cavitation on the I. T. T. C. head form at an air content ratio of $a/a_s = 0.55$.

(6a-d) Surface cleaned with acetone.

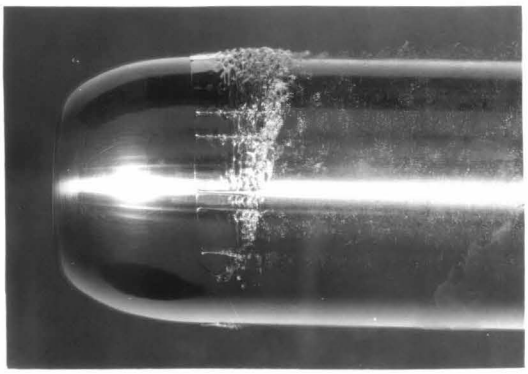

(e) V = 25.85 fps, K = 0.397

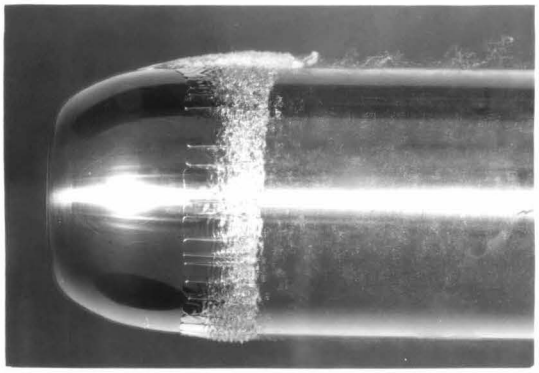

(f) V = 36.07 fps, K = 0.410

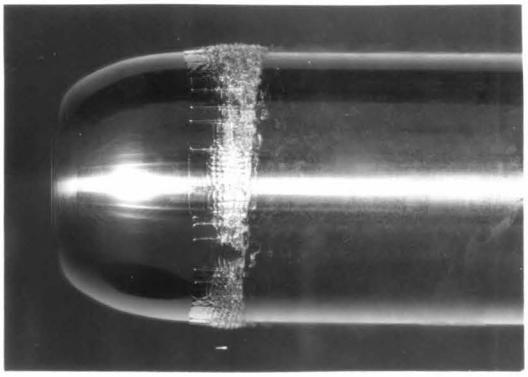

(g) V = 41.06 fps, K = 0.424

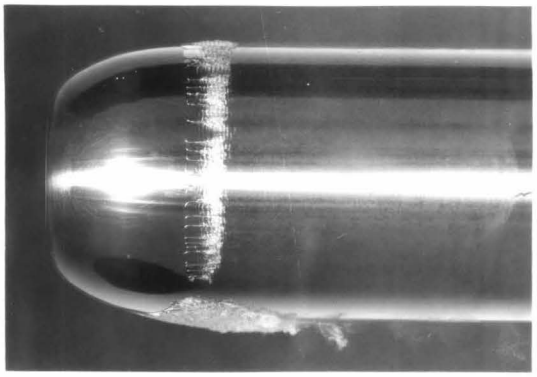

(h) V = 55.69 fps, K = 0.442

Fig. 6 - A series of photographs showing cavitation on the I. T. T. C. head form at an air content ratio of $\alpha/\alpha_s = 0.55$.

(6e-h) Surface dipped in silicone solution.

APPENDIX 1

TUNNEL CALIBRATION PROCEDURE

As there is a boundary layer growth along the walls of the working section of the tunnel, it is necessary to calibrate the tunnel both bare and with a model installed in order to determine the static pressure and the velocity head at the location of the model. Figure A-1 is a schematic diagram of the location of the pressure taps which were used to determine the distribution of static pressure down the working section. Pressure p_1 is an average of four pressure taps in the piezometer ring at the inlet of the working section. Pressure p_2 is measured just upstream of the windows of the working section; it consists of a single orifice 1/32 inch in diameter. Pressures p_3, p_4 and p_5 are taps drilled in one of the Lucite windows of the test section. These orifices are also 0.030 inches in diameter.

The tunnel calibration consists of measuring the difference between the inlet total pressure and each of the pressures p_1 through p_5. It is assumed that there is a thin boundary layer at the start of the tunnel and that the flow is sufficiently straight so that the pressure difference between the inlet total pressure and any one of the static pressures is a true measure of the dynamic pressure at that point. It is also assumed that in a bare tunnel the wall pressures are representative of the static pressure over the cross-section of the tunnel at that station. The pressure difference between the inlet total pressure and the static pressure p_1 at the inlet of the working section was measured on a mercury-water well manometer. The differences between the inlet static pressure p_1 and the other orifices, p_2 through p_5, was measured on a multi-tube water-air manometer. Each of these sets of measurements was made for tunnel speeds ranging from 25 to 50 feet per second. For these measurements the tunnel working section pressure was maintained constant at approximately 14 psig.

These pressure differences were then converted into pressure coefficients as follows:

$$C_{p_n} = \frac{p_1 - p_n}{p_t - p_1} , \qquad n = 2, 3, 4, 5 \qquad \text{(Eq. A-1)}$$

Plots of these pressure coefficients for various orifices and for velocities of 30, 40 and 50 feet per second are shown in Figure A-2. These measurements were made with the tunnel bare as mentioned and with the I.T.T.C. head form in place as indicated in Figure A-1. It can be seen from Figure A-2 that the presence of the model causes a noticeable change in the wall pressure for orifices p_4 and p_5. The change is similar at all velocities and in the worst case, for location p_5 which is very near the location of the model, it is 1.3 percent of the dynamic pressure. However, the change in the pressure at orifice p_2, which is approximately some seven model diameters upstream, due to the presence of the model is certainly less than 0.2 percent. We infer from this that the change in the static pressure at the inlet orifice p_1 is negligible.

We now list the working formulae used for the computation of tunnel speed and cavitation number:

The working formula for the computation of tunnel speed is:

$$V = \sqrt{\frac{2}{\rho}\left(p_t - p_5\right)} = \sqrt{\frac{2}{\rho}\left(p_t - p_1 + p_1 - p_5\right)}$$

This expression is now written in the form

$$V = V_{\text{manometer}} \times \sqrt{1 + C_{p_5}} \qquad \text{(Eq. A-2)}$$

where

$$V_{\text{manometer}} = \sqrt{\frac{2}{\rho}\left(p_t - p_1\right)} = \sqrt{\frac{2}{\rho}\,\Delta p}\ .$$

From Eq. A-2 it can be seen that the static pressure at orifice p_5 is used to determine the speed at the location of the model.

The calibration factor

$$\sqrt{1 + C_{p_5}} \qquad \text{(Eq. A-3)}$$

is plotted versus the pressure drop Δp expressed in feet of mercury minus feet of water in Figure A-3.

The cavitation index K in these tests is based upon vapor pressure of the fluid and the dynamic pressure at the location of the model. By

this definition

$$K = \frac{p_5 - p_v}{p_t - p_5} = \frac{p_5 - p_2 + p_5 - p_v}{p_t - p_1 + p_1 - p_5}$$

which can be written as

$$K = \frac{(p_2 - p_v)}{\Delta p(1 + C_{p_5})} + \frac{C_{p_2} - C_{p_5}}{1 + C_{p_5}} \qquad \text{(Eq. A-4)}$$

The reason that the pressure p_2 is used here is that it is the orifice that was used to determine the absolute pressure level in the tunnel working section. To aid in the calculation of the cavitation index K the following correction parameters were calculated from Figure A-2 and are plotted in Figure A-4:

$$\frac{C_{p_2} - C_{p_5}}{1 + C_{p_5}} \qquad \text{(Eq. A-5)}$$

$$\frac{1}{1 + C_{p_5}} \qquad \text{(Eq. A-6)}$$

In preparing these graphs and in determining these calibration factors the pressure coefficients used from Figure A-2 are those corresponding to the bare tunnel. Thus no account of the tunnel blockage is made in determining either the cavitation parameters or the tunnel speed.

List of Figures

Fig. A-1 Schematic diagram of three-dimensional working section showing location of pressure taps and model.

Fig. A-2 Dimensionless pressure coefficients versus distance from inlet to working section for various velocities.

Fig. A-3 Calibration factor Eq. A-3 versus pressure drop across the nozzle.

Fig. A-4 Calibration factors Eqs. A-5 and A-6 versus pressure drop across the nozzle.

PRESSURE TAP LOCATION

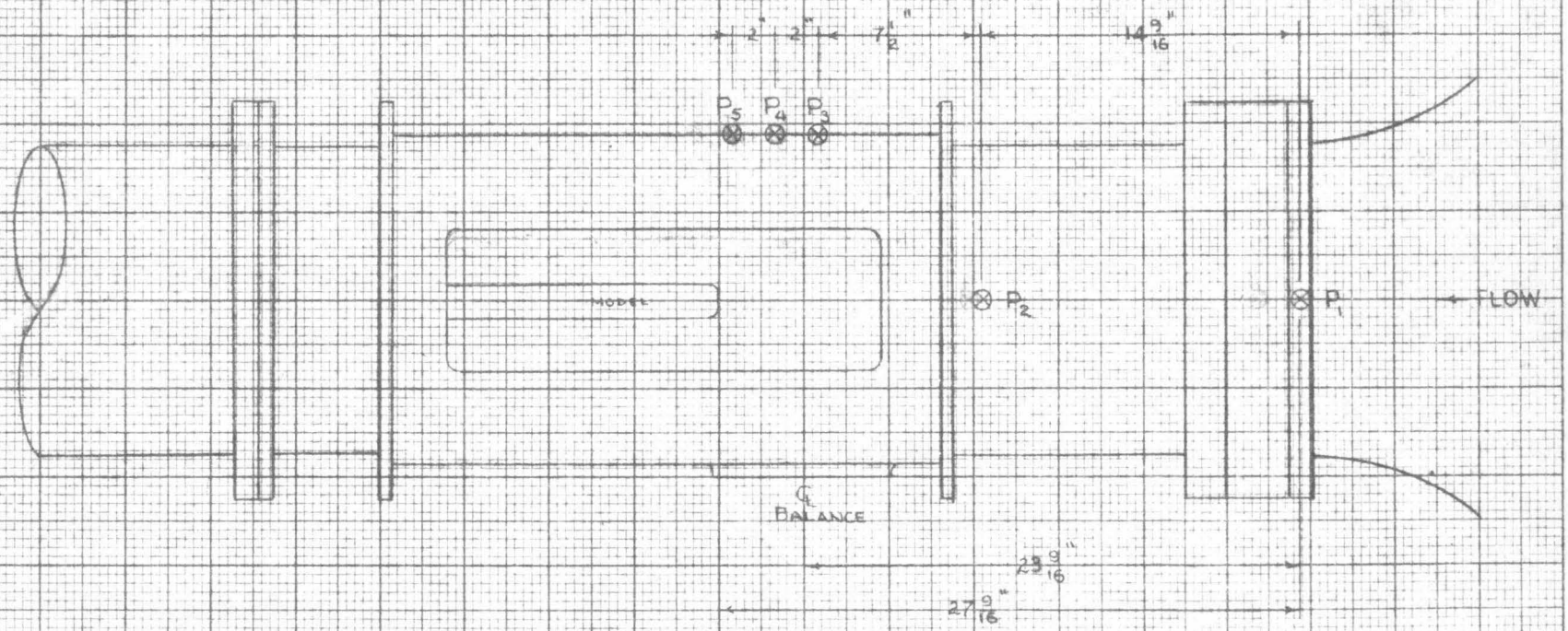

P_1 — $\frac{3}{32}$" DIAM.

$P_2 - P_5$ — $\frac{1}{32}$" DIAM.

Fig. A-1

5 SEPT. 1966
MTH

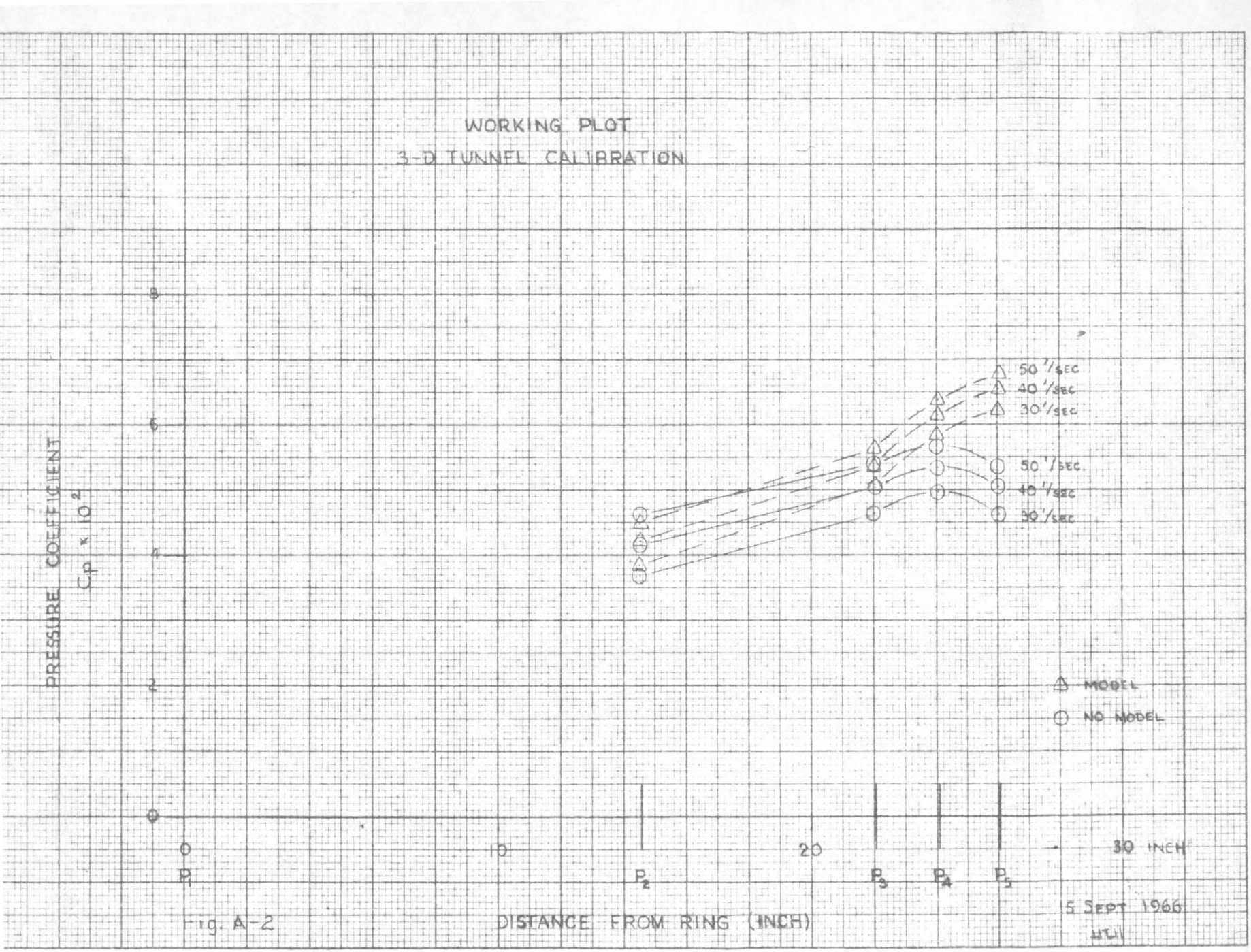
WORKING PLOT
3-D TUNNEL CALIBRATION
PRESSURE COEFFICIENT
$C_p \times 10^2$
8
6
4
2
0
50 '/SEC
40 '/SEC
30'/SEC
50 '/SEC.
40 '/SEC
30'/SEC
MODEL
NO MODEL
0
10
20
30 INCH
P_1
P_2
P_3
P_4
P_5
DISTANCE FROM RING (INCH)
5 SEPT 1966
HTL

Fig. A-2

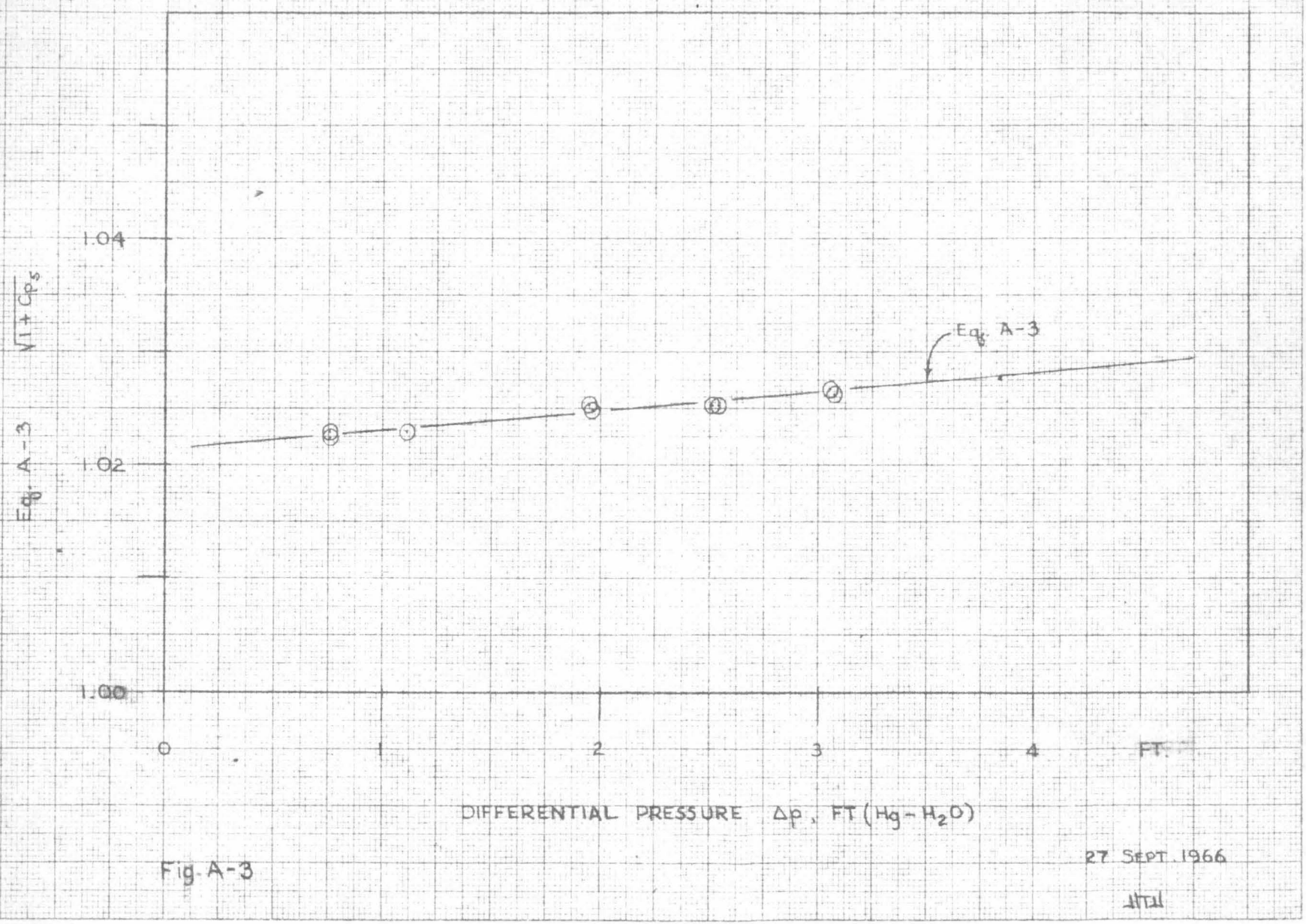

Fig. A-3

27 SEPT. 1966

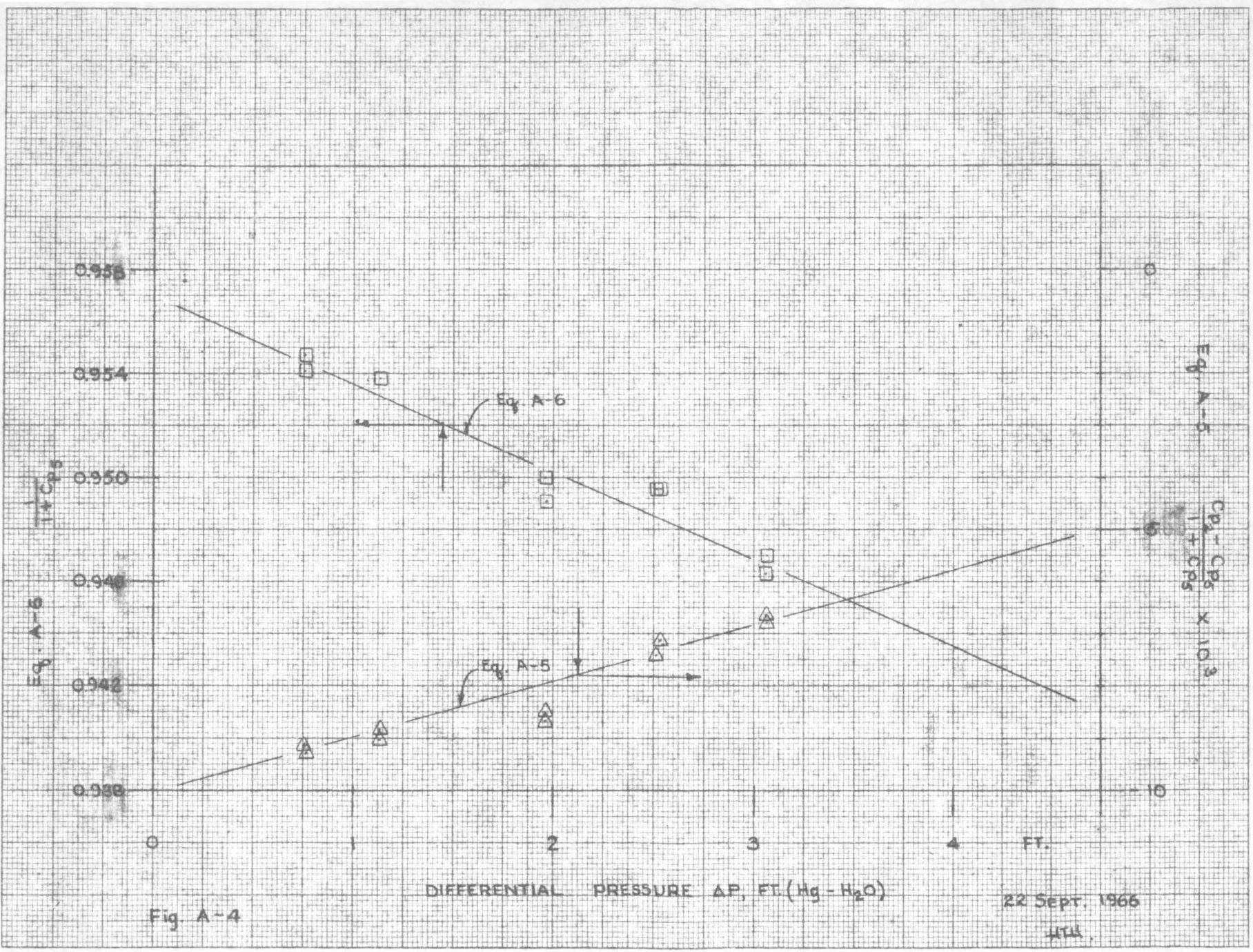

Fig. A-4

22 Sept. 1966

HTH.